
This manuscript is a preprint and has been submitted for publication. Please note that, despite having undergone peer-review, the manuscript has yet to be formally accepted for publication. Subsequent versions of this manuscript may have slightly different content. If accepted, the final version of this manuscript will be available via the 'Peer-reviewed Publication DOI' link on the right-hand side of this webpage. Please feel free to contact any of the authors; we welcome feedback.

A minimally cemented shallow crust beneath InSight

Vashan Wright¹, Jhardel Dasent¹, Richard Kilburn¹, and Michael Manga²

¹University of California San Diego, Scripps Institution of Oceanography, La Jolla, CA, 92037

²University of California Berkeley, Department of Earth and Planetary Science, Berkeley, CA, 94720

Key Points:

- Any significant volumes of ice or mineral cements within the upper 300 m beneath InSight are likely nodular or broken.
- No ice- or liquid water-saturated layers were seismically resolved within the upper 300 m beneath InSight.
- Fractures in basalt layers within the upper 300 m beneath InSight could host up to 20 volume percent ice.

Corresponding author: Vashan Wright, vwright@ucsd.edu

12 Abstract

13 Ice and other mineral cements in Mars' shallow subsurface affect the mechanical
14 properties of the shallow crust, the geologic processes that shape the planet's surface,
15 and the search for past or extant Martian life. Cements increase seismic velocities. We
16 use rock physics models to infer cement properties from seismic velocities. Model results
17 confirm that the upper 300 m of Mars beneath InSight is most likely composed of sedi-
18 ments and fractured basalts. Grains within sediment layers are unlikely to be cemented
19 by ice or other mineral cements. Hence, any existing cements are nodular or formed away
20 from grain contacts. Fractures within the basalt layers could be filled with gas, 2% min-
21 eral cement and 98% gas, and no more than 20% ice. Thus, no ice- or liquid water-saturated
22 layers likely exist within the upper 300 m beneath InSight. Any past cement at grain
23 contacts has likely been broken by impacts or marsquakes.

24 Plain Language Summary

25 High priority Mars exploration goals are to determine if Mars ever supported life,
26 to understand its climate history, to understand Mars as a geological system, and to pre-
27 pare for human exploration. A key step towards these goals is understanding how much
28 ice and other minerals fill pores and fractures within the Martian subsurface and cement
29 grains or pieces of rocks together. The InSight lander on Mars has an instrument whose
30 data provide estimates for the velocity of seismic waves within the crust. These veloc-
31 ities change depending on rock type and the material that fills the pores and fractures
32 within rocks. Possible pore-filling materials include gas, liquid water, ice, and other min-
33 eral cements. We find that the shallow crust is at best weakly cemented and the pores
34 within the rocks are not entirely filled with ice or liquid water.

35 1 Introduction

36 Cements in the Martian crust can have multiple origins, including ice frozen from
37 liquid water or condensed from vapor, hydrated minerals formed in situ, or minerals pre-
38 cipitated from aqueous fluids (e.g., salts, carbonates, and sulphates). The presence, amount,
39 and composition of ice and other mineral cements in the shallowest sections of the Mar-
40 tian crust have implications for robotic and human exploration of Mars, the processes
41 that shape and shaped the surface, and the search for past or extant life. These topics
42 are central to the four overarching goals of the Mars Exploration Program Analysis Group
43 to determine if Mars ever supported life, to understand the climate history and processes,
44 to understand Mars as a geological system, and to prepare for human exploration.

45 Cementation affects and records geological processes. Cement can strengthen sedi-
46 ments (herein defined to include regolith and all other granular media layers) by cre-
47 ating stiffer contacts between particles. Cementation affects permeability and porosity
48 of sediments and fractured rocks, which impacts gas transport driven by atmospheric pres-
49 sure changes (Morgan et al., 2021). Pores and fractures filled with ice or other mineral
50 cement could confine any deeper liquid water, creating aquifers (Carr, 1979). Ground
51 ice can promote weak explosive eruptions at rootless cones on lava flows (Brož et al., 2021)
52 and may promote phreatomagmatic eruptions (Moitra et al., 2021). Cemented sediments
53 are less prone to eolian and fluvial transport and erosion. Hence, the distribution of ce-
54 ments in the Martian sediments may record the accumulation and transport of volatiles
55 in geologically recent times (Dundas et al., 2021). The present or past habitability of icy
56 sediments and fractured rocks alongside any associated brines may be recorded by or-
57 ganic compounds diagnostic of past or present biological activity (Rivera-Valentín et al.,
58 2020).

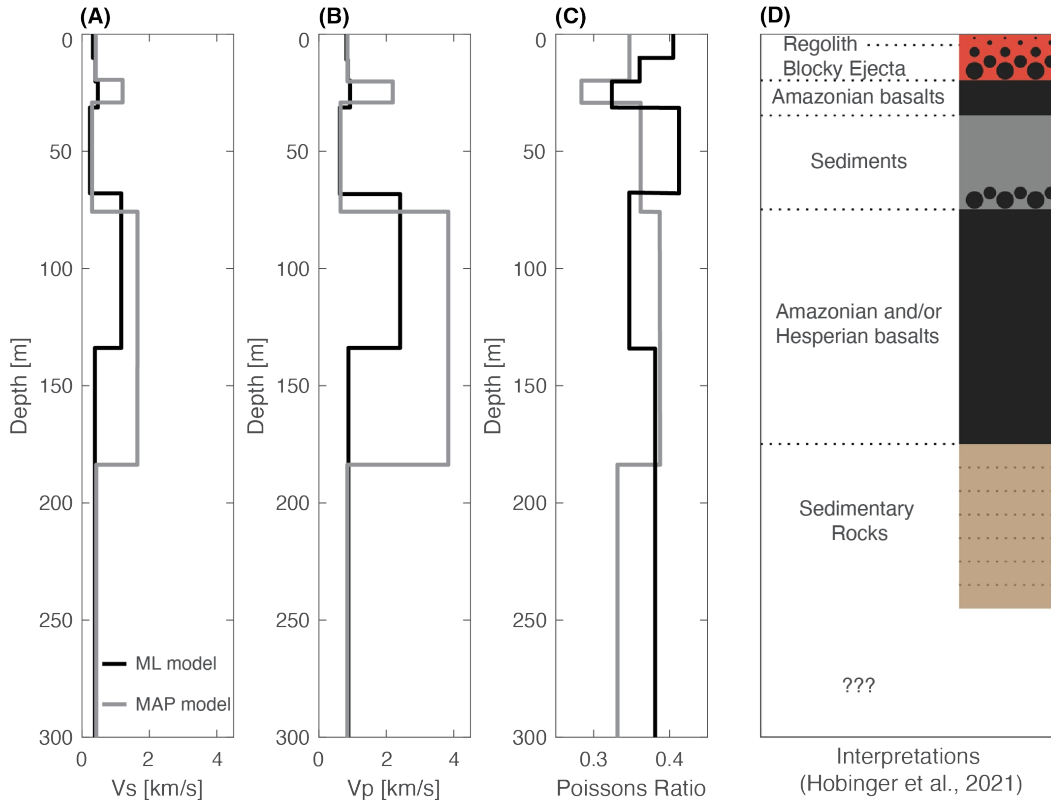


Figure 1. Models of (A) V_s and (B) V_p from Hobiger et al. (2021) and (C) calculated Poisson ratio based on the seismic velocities. The black and grey curves are Hobiger et al. (2021)’s maximum likelihood (ML) and maximum a posteriori (MAP) models, respectively. (D) Inferred stratigraphy of the upper 300 m beneath InSight, from Hobiger et al. (2021).

59 Cementation impacts human exploration and a primary motivation for the Mars
 60 Ice Mapper mission concept is to map ice in the shallowest crust (Davis & Haltigin, 2021).
 61 The presence of ice and hydrated minerals in shallow sediments and fractured rocks could
 62 provide a source of water for in situ resource utilization (Piqueux et al., 2019). Cementation-
 63 induced strengthening of sediments affects foundations used for engineering infrastruc-
 64 ture (Kalapodis et al., 2020). Cemented sediments can be used as a construction ma-
 65 terial (Liu et al., 2021) and has prompted studies of a range of Mars simulants in prepa-
 66 ration for future human missions (Karl et al., 2021). Efforts to map and study shallow
 67 subsurface ice and other mineral cements integrate complementary insights from direct
 68 and indirect observations. Direct, in situ measurements of ice and other mineral cements
 69 at specific landing sites is possible, yet sometimes challenging. The Phoenix lander ex-
 70 cavated ice in the upper few cm (Morgan et al., 2021). At the InSight (Interior Explora-
 71 tion using Seismic Investigations, Geodesy, and Heat Transport mission) landing site,
 72 where eolian processes and impact brecciation created a 10-30 m thick regolith whose
 73 upper approximately 3 m is a sand horizon (Golombek et al., 2020; Warner et al., 2022),
 74 the rover had difficulties penetrating its heat flow probe (HP3) into the subsurface owing
 75 to insufficient friction (Spohn et al., 2021). Indirect methods of detecting ice and other
 76 mineral cements include analyses of neutron detection, thermal inertia, geomorphic, and
 77 radar data (Morgan et al., 2021). Other indirect methods exploit the sensitivity of ge-
 78 omechanical properties to cements, which influence geophysical properties such as seis-
 79 mic velocity, electrical conductivity, and gravity. For example, Manga and Wright (2021)

80 used seismic velocities interpreted with rock physics models to infer that there is likely
 81 no ice-saturated cryosphere in the 0 to 7.5 km depth range beneath the InSight land-
 82 ing site, though some mineral cement could be present at greater depths.

83 Here we study the presence and quantity of mineral and ice cements in the upper
 84 300 m of the Martian crust by interpreting seismic velocity models derived from data
 85 collected by the seismometer deployed by the InSight lander. We interpret the seismic
 86 velocities using rock physics models and a theoretical relationship between dry-frame Pois-
 87 son’s ratio and grain contact forces. Figure 1 based on results from Hobiger et al. (2021)
 88 shows their derived seismic velocities beneath InSight and the inferred stratigraphy and
 89 lithology. Shear wave velocities V_s generally increase from ~ 0.3 km/s at the surface to
 90 ~ 1.7 km/s at 175 m; compressional wave velocities V_p increase from ~ 0.8 m/s to ~ 3.8
 91 km/s within the same depth. At least two low velocity zones exist from 0-157 m and 175-
 92 300 m, where V_s decreases to ~ 0.4 km/s and V_p decreases to ~ 0.8 - 0.9 km/s. Hobiger
 93 et al. (2021) interpreted the higher and lower velocity layers as fractured basalts and sed-
 94 iment, respectively (Figure 1D), consistent with geological mapping (Warner et al., 2022).
 95 Our interpretations of these seismic velocities are that sediment within the upper 300
 96 m of the Martian crust is gas-filled, mineral or ice cements likely do not exist at grain
 97 contacts, and there is no evidence for any ice-saturated cryosphere.

98 2 Methods

99 2.1 Inferring Subsurface Properties Using Rock Physics Models

100 We compare measured with theoretically modeled V_s and V_p to infer the mechanical
 101 properties of the upper 300 m beneath InSight, constraining uncertainties with Monte
 102 Carlo analyses. For sediments, we assume a porosity reduction profile for Mars, predict
 103 seismic velocities with that assumed profile, then compare modeled to measured veloc-
 104 ities. For fractured basalt layers, we created rock physics templates that relate seismic
 105 velocities, porosity (0-50%), and fracture shape represented by elliptical inclusions with
 106 aspect ratio, defined as the inclusion shape’s short axis divided by long axis, $\alpha = 0.01$ -
 107 1. We used the templates to identify the combinations of porosity and fracture shapes
 108 that could explain both measured V_p and V_s .

109 We compute V_s and V_p from

$$V_s = \sqrt{\frac{\mu_e}{\rho}} \quad (1)$$

$$V_p = \sqrt{\frac{\kappa_e + \frac{4}{3}\mu_e}{\rho}} \quad (2)$$

110 where ρ , κ_e , and μ_e are bulk density, effective bulk modulus, and effective shear mod-
 111 ulus, respectively. Bulk density ρ is

$$\rho = (1 - \phi)\rho_m + \phi\rho_f \quad (3)$$

112 where ρ_f and ρ_m are fluid and mineral densities, respectively.

113 Rock physics theoretical models predict dry-frame shear and bulk moduli (μ and
 114 κ); $\mu_e = \mu$ and $\kappa_e = \kappa$ for dry rock (Gassmann, 1951; Biot, 1956). We use Hertz-Mindlin’s
 115 (Mindlin, 1949) rock physics models for uncemented sediments. We use the contact ce-
 116 ment model (Dvorkin & Nur, 1996) for sediments with cement that completely surrounds
 117 grains that are in contact or cement that only exists at grain contacts. We use the Berry-

118 man self-consistent model (Berryman, 1980) for fractured rocks. The equations for the
 119 rock physics models are in Mindlin (1949), Dvorkin and Nur (1996), and Berryman (1980).

120 We use Gassmann-Biot fluid substitution theory (Gassmann, 1951; Biot, 1956) to
 121 calculate effects of fluid saturation on κ (i.e., κ_e for liquid water saturated rocks),

$$\frac{\kappa_e}{\kappa_m - \kappa_e} - \frac{\kappa_{f2}}{\phi(\kappa_m - \kappa_{f2})} = \frac{\kappa}{\kappa_m - \kappa} + \frac{\kappa_{f1}}{\phi(\kappa_m - \kappa_{f1})} \quad (4)$$

122 where κ_{f2} , κ_m , and κ_{f1} are the bulk moduli of the saturating fluid (liquid water in our
 123 case), mineral(s), and gas (0 kPa), respectively. Gassmann-Biot theory assumes that flu-
 124 ids are not flowing and minerals and fluids homogeneously distribute within rocks (Gassmann,
 125 1951; Biot, 1956).

126 The models' input parameters are porosity ϕ , coordination number c_n (average num-
 127 ber of grains in contact), effective pressure P , mineral Poisson's ratio ν_m , cement frac-
 128 tion c_f , cement bulk κ_m and shear μ_m moduli, pore aspect ratio α , and grain roughness
 129 fraction f (i.e., percentage of grain contacts that allows tangential slip, which we assume
 130 to be 0 % or 100 % to model end-member ranges). We assumed porosity ϕ at the sur-
 131 face (critical porosity ϕ_c) is between 0.3 and 0.5 (Golombek et al., 2018; Lewis et al., 2019;
 132 Smrekar et al., 2019; Lognonné et al., 2020) and that ϕ exponentially decays with depth
 133 z ,

$$\phi = \phi_c e^{-\frac{z}{k}} \quad (5)$$

134 where k is a compaction constant (2.82 km) scaled to Mars' gravitational field (Clifford,
 135 1986). Effective pressure P is

$$P = \rho gh - p_f \quad (6)$$

136 where g , h , and p_f represent Mars' gravitational acceleration (3.71 m/s²), depth, and
 137 fluid pressure, respectively. We constrain coordination number c_n empirically (Murphy,
 138 1982)

$$c_n = 20 - 34\phi + 14\phi^2. \quad (7)$$

139 The minerals that we use in models and their respective κ_m and μ_m in GPa are calcite
 140 cement (71.6 and 28.2), basalt grains and rocks (80.0 and 40.0), and ice cement (3.7 and
 141 3.8) (Vanorio et al., 2003; Zong et al., 2017). These are some of the main minerals ex-
 142 pected within the upper 300m of the Martian crust (Tanaka et al., 2014; Golombek et
 143 al., 2018; Pan et al., 2020). We calculated Poisson ratio from

$$\nu_m = \frac{3\kappa_m - 2\mu_m}{6\kappa_m + 2\mu_m}. \quad (8)$$

144 We used Monte Carlo analyses to constrain the effects of input parameter uncer-
 145 tainties on the velocities predicted by the rock physics model for cemented and uncemented
 146 sediments. In each of our 10,000 realizations, we randomly generated and used a new
 147 input parameter value between their ranges. We generate new ϕ -depth profiles from the
 148 selected ϕ_c . Coordination numbers, bulk densities, and effective pressures change with
 149 ϕ -depth profiles.

150 2.2 Inferring Subsurface Properties From Poisson's Ratio

151 We infer the volume fraction of cemented grain contacts from the relationship be-
 152 tween Poisson's ratio and the volume fraction of rough versus smooth grain contacts f .
 153 Rough (smooth) grain contacts resist (allow) elastic tangential grain contact slip dur-
 154 ing seismic wave propagation. We conjecture that, in the absence of cemented grains,

155 Martian sediments comprise nearly 100% smooth grain contacts. We make this con-
 156 jecture because Mars’ gravitational acceleration (3.7 m/s^2) is lower than Earth’s (9.8 m/s^2).
 157 Gravitational acceleration impacts grain contact forces significantly (Equation 6). As-
 158 suming 100% smooth grain contacts routinely results in better seismic velocities predic-
 159 tions in shallow sediments on Earth (Buckingham, 2000; Zimmer et al., 2007; Majmu-
 160 dar & Behringer, 2005; Wright & Hornbach, 2021) and low friction grain contacts pre-
 161 vented InSight’s heatflow probe from penetrating the shallow subsurface. Given the as-
 162 sumptions, conjectures, and expectations mentioned, cements are likely one of the main
 163 causes for rough grain contacts, making f synonymous with the volume of cemented grain
 164 contacts in those cases. We can compute ν_d from ν_m and f for an aggregate of identi-
 165 cal perfect spheres (Walton, 1987; Bachrach & Avseth, 2008)

$$\nu_d = \frac{(2 - \nu_m)}{4(2 - \nu_m) + 2f(1 - \nu_m)} - \frac{2f(1 - \nu_m)}{4(2 - \nu_m) + 2f(1 - \nu_m)}. \quad (9)$$

166 f decreases as ν_d increases (Walton, 1987). We compute ν_d from the measured V_p and
 167 V_s

$$\nu_d = \frac{1}{2} \frac{(V_p/V_s)^2 - 2}{(V_p/V_s)^2 - 1}. \quad (10)$$

168 Our calculation assumes that there is no liquid water within the sediment layers.

169 3 Results

170 3.1 Inferred Pore-Filling Media in Sediments

171 The sediments most likely host grains that experience relatively low friction at con-
 172 tacts. Low friction is indicated by the observation that smooth-grained models produce
 173 better seismic velocity predictions (i.e., lower misfits) than rough-grained models, regard-
 174 less of assumed pore-filling material (Figure 2). The differences between smooth- versus
 175 rough-grain model predictions are 0.3-0.4 km/s and 0.1-0.5 km/s for V_s and V_p , re-
 176 spectively. Low friction is also indicated by the Poisson’s ratio for sediment layers, 0.33-
 177 0.41 (Figure 1). These Poisson’s ratio values result in negative values (-0.55 to -0.10) for
 178 the calculated volume fraction of rough grains (equation 10), which indicates that there
 179 are likely no rough grain contacts present, that the model breaks down for such high val-
 180 ues, or both.

181 The pores are most likely filled with gas (Figure 2). Modeled smooth-grained V_s
 182 for gas and liquid water-filled pores are within 0-0.1 km/s of measured V_s . Modeled V_p
 183 are within 0.01-0.05 km/s of measured V_p , assuming that gas fills the pores; assuming
 184 100% liquid water in the pores results in V_p overprediction by 0.6-1.0 km/s. Models that
 185 assume pores are filled with 2% cement overpredict V_p and V_s by 2.5-4.0 km/s. Assum-
 186 ing that ice fills the pores results in V_p and V_s overpredictions by 2.0-2.3 km/s and 2.7-
 187 3.0 km/s, respectively for the sediments.

188 3.2 Inferred Pore-Filling Media in Fractured Basalts

189 The hypothesized fractured basalt layers could host 100% gas, 100% liquid water,
 190 2% calcite cement and 98% air, and 2% calcite cement and 98% water in the fractures;
 191 hosting 100% ice is unlikely. A gas-filled basalt requires the narrowest range of aspect
 192 ratio and porosity combination to be consistent with the measured seismic velocities. A
 193 liquid water-filled basalt is consistent with the measured seismic velocities if the basalts’
 194 porosities are between 0.13 and 0.47 for aspect ratios between 0.03 and 1; aspect ratios
 195 increase with increasing porosities. A basalt hosting 2% calcite cement and 98% gas or
 196 liquid water in its fractures could explain the measured velocities if the porosities are
 197 0.24-0.5. The range of possible aspect ratios increase with increasing porosities. All com-
 198 binations of porosities and aspect ratios for a 100% ice-filled basalt results in velocities

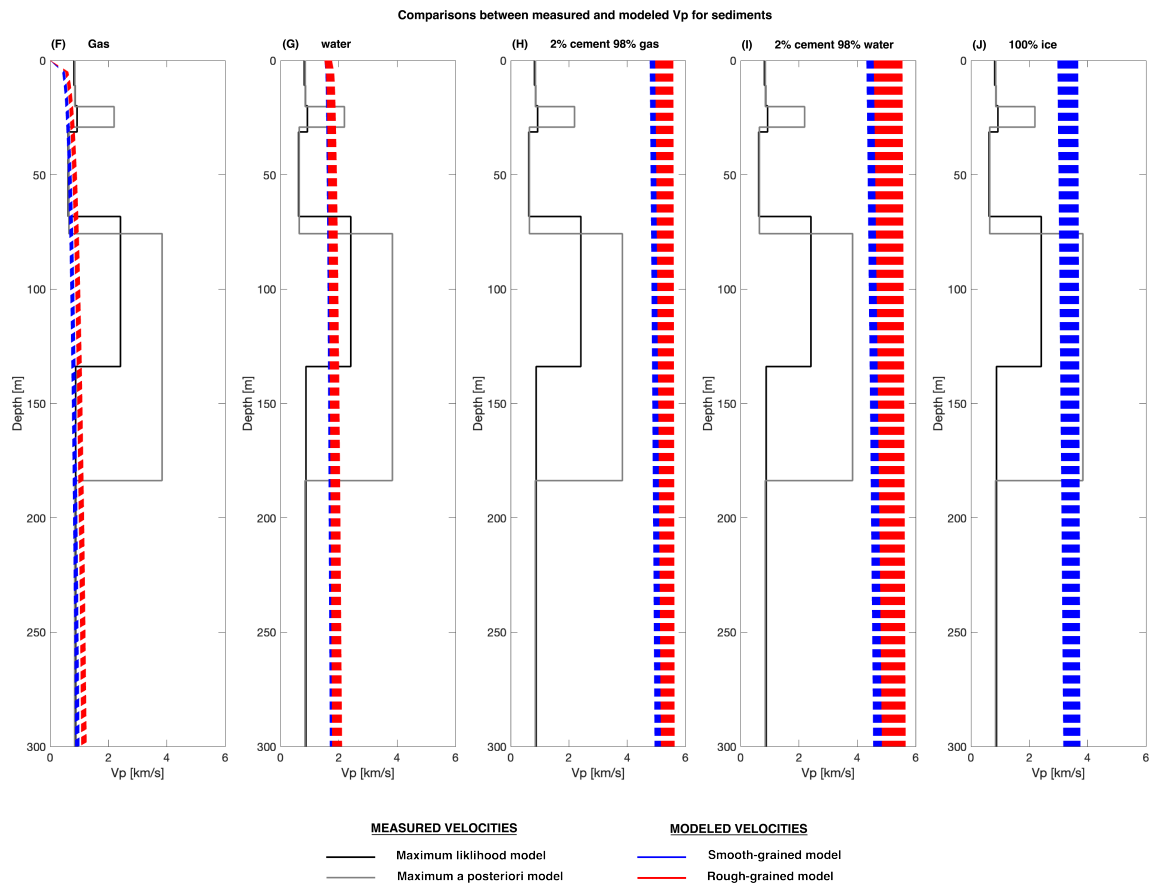
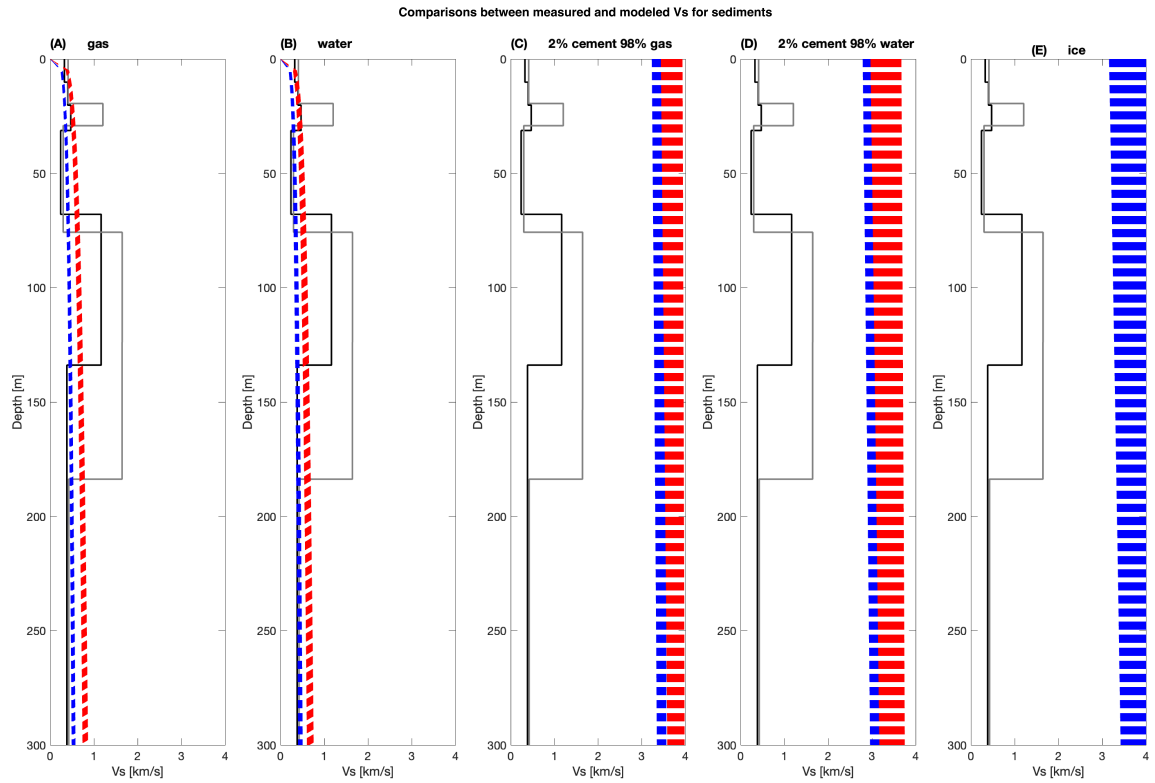


Figure 2. Measured V_p and V_s (black and grey lines) compared to model predicted V_p and V_s for sediment whose pores are filled with gas, liquid water, 2% calcite cement and 98% gas, 2% calcite cement and 98% liquid water, and ice. Blue and red lines are the smooth-grained and rough-grained model results, respectively.

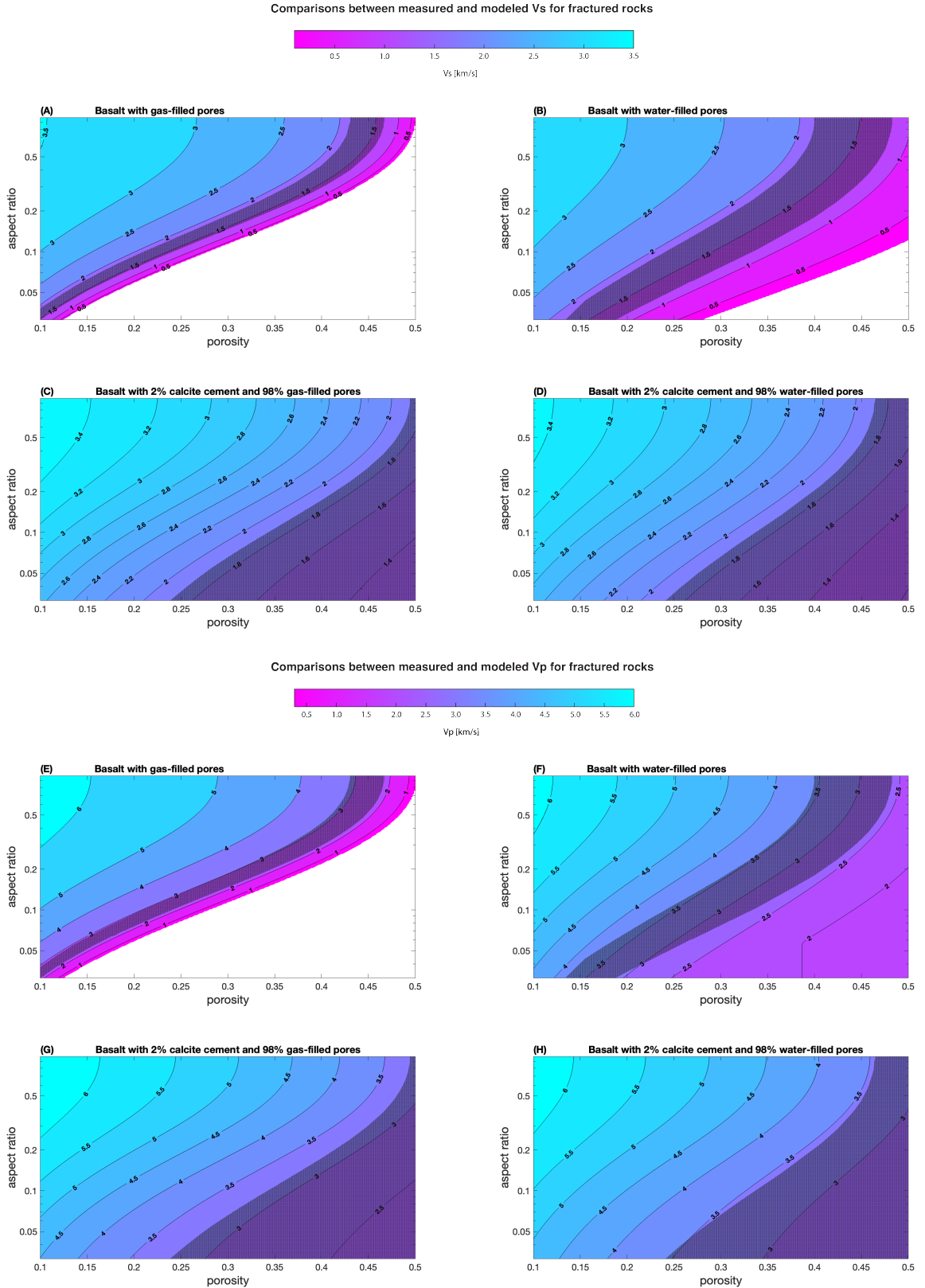


Figure 3. Rock physics model templates showing predicted V_s and V_p for a fractured basalt with various pore filling materials. Shaded regions are the combinations of modeled velocities, porosities, and aspect ratios that match both the measured V_p and V_s . Vertical scale is logarithmic.

199 that are 1.1-2.8 times higher than measured. Thus, measured V_s and V_p are too low for
200 an 100% ice-filled fractured basalt.

201 4 Discussion

202 We now discuss our most robust interpretations for the distribution of cements within
203 the upper 300 m beneath InSight, considering the model assumptions and limitations.
204 The cemented and uncemented granular media models assume that grains are identical
205 spheres experiencing equal contact forces, which are idealizations for Martian and other
206 sediments (Makse et al., 1999, 2004; Day-Lewis et al., 2005; Majmudar & Behringer, 2005;
207 Bachrach & Avseth, 2008). These model assumptions sometimes lead to overpredictions
208 in low effective stress environments on Earth (Buckingham, 2000; Zimmer et al., 2007;
209 Majmudar & Behringer, 2005; Wright & Hornbach, 2021). The cementation models pre-
210 dict elastic moduli by homogeneously distributing the entire volume of cement within
211 the sediments, which may also be too idealistic for actual sediments (Dvorkin & Nur,
212 1996). Considering the model limitations, we can still make two main interpretations:
213 any shallow cements in Martian sediments likely do not adhere grains, and pores within
214 the layers are not filled with liquid water or ice.

215 4.1 Basalt with up to 20% of its pores filled with ice

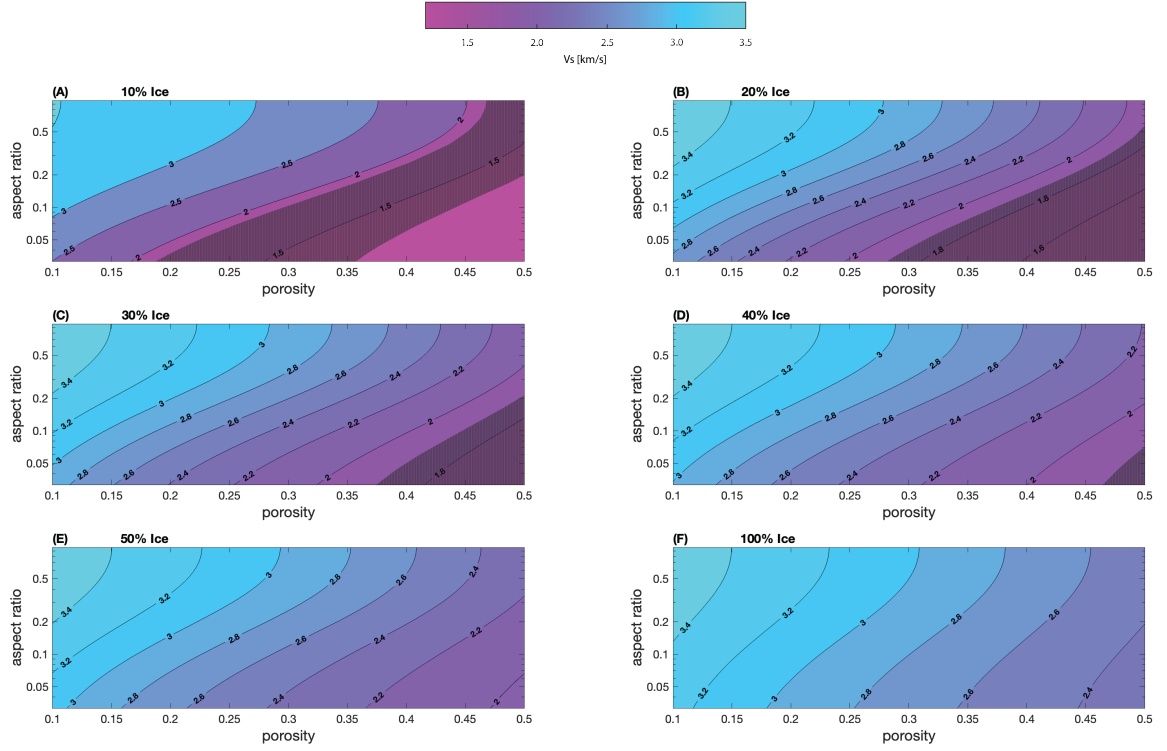
216 A seismically detectable cryosphere likely does not exist within the upper 300 m
217 beneath InSight. This is indicated by the observation that the granular and fractured
218 media models predict velocities that are too high for fully ice-saturated sediments and
219 basalt. It is unlikely that a basalt layer has been misinterpreted for an ice-saturated sed-
220 iment layer; the predicted V_p for the Amazonian and/or Hesperian basalt layer matches,
221 but V_s is overpredicted by at least 1.4-1.5 km/s (Figures 1-2). A partial cryosphere, with
222 up to 20% ice, could exist in the fractured basalt layers. Though the measured veloc-
223 ities are consistent with modeled velocities for a fractured basalt whose pores are filled
224 with up to 40% ice, porosities of basaltic lava flows rarely reach such high values except
225 in thin horizons where vesicles accumulate (Cashman & Kauahikaua, 1997) or when chem-
226 ical reactions alter the minerals within the basalt and lead to higher porosities (Franzson
227 et al., 2010; Broglia & Ellis, 1990). Moreover, estimated and modelled porosity for ex-
228 posed Martian basalts and meteorites are less than 40% (Hanna & Phillips, 2005; MacK-
229 innon & Tanaka, 1989). Limiting the range of porosity to up to 40% then implies that
230 measured velocities are only consistent with a basalt with less than 20% of the pores filled
231 with ice. We did not model the effects of salinity on ice and seismic velocities; increased
232 salinity may lead to mushy ice in the pores and reduce seismic velocities, depending on
233 the temperatures and wetting behavior (Dou et al., 2017). Future studies could explore
234 this possibility.

235 Our inferences are consistent with findings from the Mars Subsurface Water Ice Map-
236 ping (SWIM) project, which used neutron detection, thermal inertia, geomorphology, radar
237 surface mapping, and radar dielectric analysis to search for shallow subsurface ice (Morgan
238 et al., 2021). The SWIM data compilation suggests that shallow ice is unlikely to be present
239 at the near-equatorial landing site of InSight, 4.5 °N. SWIM is most sensitive to the up-
240 per few meters. Thus, our finding that the shallowest sediment layer, which extends to
241 20-70 m, likely does not contain ice that cements grains is consistent with results from
242 the SWIM project. Importantly, the SWIM data does not provide additional constraints
243 on the basalt layers since the SWIM data are not sensitive to those depths.

244 4.2 Mineral cements as framework grains

245 Most mineral cements, if they exist, likely do not adhere grains substantially. One
246 support for this interpretation comes from the observation that there are likely no sig-

Comparisons between measured and modeled V_s for basalt with ice in its pores



Comparisons between measured and modeled V_p for basalt with ice in its pores

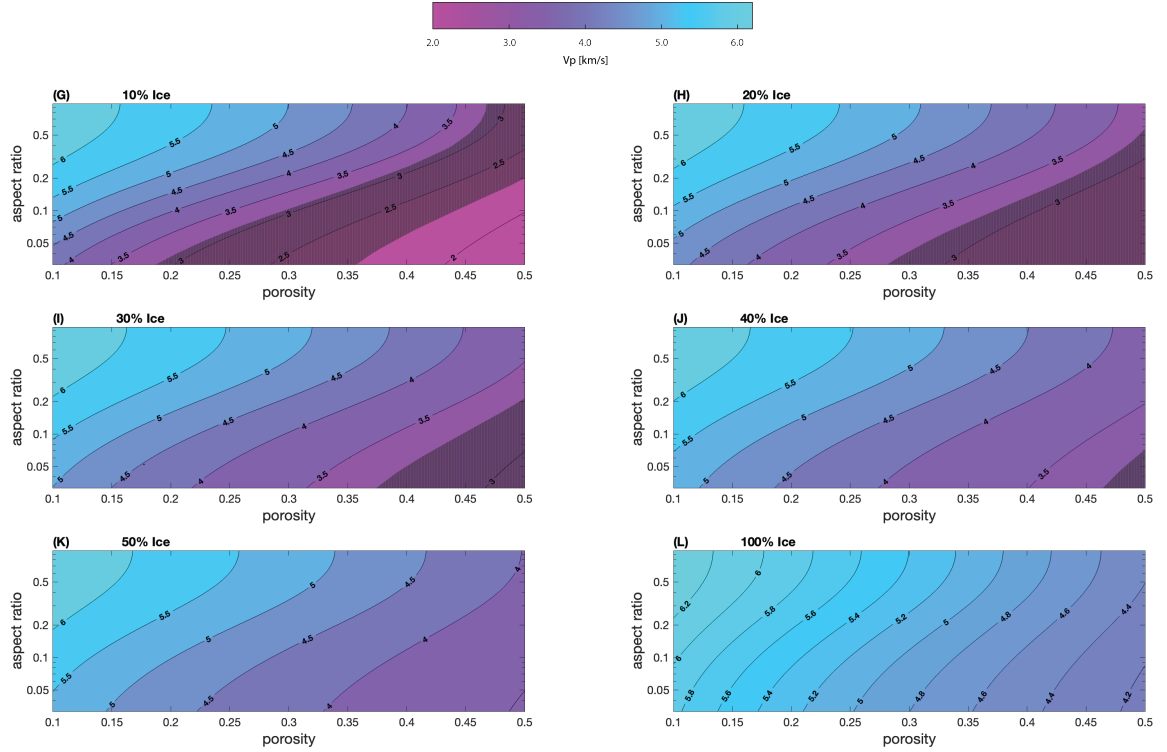


Figure 4. (A-I) Rock physics model templates showing predicted V_s and V_p for a fractured basalt with varying percentage of ice within the fractures. Shaded regions are the combinations of modeled velocities, porosities, and aspect ratios that match both measured V_s and V_p from Hobiger et al. (2021). Vertical scale is logarithmic.

nificant volumes of rough grain contacts in sediments, as indicated by the high Poisson's ratios. Additional support comes from the observation that the models with calcite cement at grain contacts and surrounding the grains overpredict V_p and V_s by 2.5-4.0 km/s. Other mineral cements (e.g., clay and quartz cements) also likely do not adhere grains since the differences in the elastic moduli between calcite and other mineral cements would not lead to a 2.5-4.0 km/s increase in seismic velocities. Nodular cements and concretions that are a part of the network of framework grains or cements that form on grains without adhering to other grains, could exist. These cement types would produce roughly the same seismic velocities as gas-filled sediment with the same porosity. Thus, any existing cements likely resulted from mineral alteration, such as hydrating minerals (Scheller et al., 2021; Wernicke & Jakosky, 2021), precipitating salts (Sun et al., 2019), or the formation of concretions or spherules (Squyres et al., 2004, 2006).

Cements could have formed at the grain contacts of Martian sediments, only to be later broken by impacts and strong marsquakes. Impacts that formed basins 200-600 km in diameter create dynamics strains similar to magnitude 10 and 11 quakes and could disrupt sediment globally on Mars (Clifford, 1997; Wang et al., 2005). The forces from these impacts are likely strong enough to break cemented bonds since laboratory experiments show that, depending on the porosity of the sediments and degree of cementation (weak or strongly cemented), the relatively low strain rates from cyclic shearing (i.e., the type of waves experienced during seismic events) can break weakly cemented bonds (Sharma & Fahey, 2003; Zeghal & El Shamy, 2008; Suzuki et al., 2012; Suazo et al., 2017).

5 Conclusions

The presence, volume, and distribution of ice and other mineral cements in Martian sediments and fractured rocks may record and affect geologic processes. Seismic velocities are sensitive to cement properties and rock physics models provide one approach to relate cement properties to seismic velocities. Using these models to interpret seismic velocities derived from InSight data, we find that any cement within the upper 300 m beneath InSight likely does not cement grain contacts in sediments. An ice-saturated cryosphere likely does not exist, but fractured basalts whose pores contain up to 20% ice is possible. The findings support ideas that some of Mars' past surface liquid water could be incorporated in cements that resulted from mineral alteration, precipitating salts, or the formation of concretions or spherules. Any cement at grain contacts was likely either weak and perhaps broken by impacts or marsquakes. Future studies could revisit these inferences as more constraints become available on the porosity, mineralogy, lithology, density, seismic velocity, and heat flow within the shallowest sections of the Martian crust.

6 Data Availability Statement

No data was used in this study.

Acknowledgments

Thanks to NASA and the InSight team for their vision, hard work, and dedication, especially during this time when Covid-19 is real. V. Wright, J. Dasent, and R. Kilburn acknowledge support from NSF grant EAR2136301. M. Manga acknowledges support from NASA grant 80NSSC19K0545 and the CIFAR Earth 4D program.

References

Bachrach, R., & Avseth, P. (2008). Rock physics modeling of unconsolidated sands: Accounting for nonuniform contacts and heterogeneous stress fields in the ef-

- 293 fective media approximation with applications to hydrocarbon exploration.
294 *Geophysics*, 73(6), E197–E209.
- 295 Berryman, J. G. (1980). Long-wavelength propagation in composite elastic media ii.
296 ellipsoidal inclusions. *The Journal of the Acoustical Society of America*, 68(6),
297 1820–1831.
- 298 Biot, M. A. (1956). Theory of propagation of elastic waves in a fluid-saturated
299 porous solid. ii. higher frequency range. *The Journal of the acoustical Society*
300 *of america*, 28(2), 179–191.
- 301 Broglia, C., & Ellis, D. (1990). Effect of alteration, formation absorption, and stand-
302 off on the response of the thermal neutron porosity log in gabbros and basalts:
303 Examples from deep sea drilling project-ocean drilling program sites. *Journal*
304 *of Geophysical Research: Solid Earth*, 95(B6), 9171–9188.
- 305 Brož, P., Bernhardt, H., Conway, S. J., & Parekh, R. (2021). An overview of explo-
306 sive volcanism on mars. *Journal of Volcanology and Geothermal Research*, 409,
307 107125.
- 308 Buckingham, M. J. (2000). Wave propagation, stress relaxation, and grain-to-grain
309 shearing in saturated, unconsolidated marine sediments. *The Journal of the*
310 *Acoustical Society of America*, 108(6), 2796–2815.
- 311 Carr, M. H. (1979). Formation of martian flood features by release of water from
312 confined aquifers. *Journal of Geophysical Research: Solid Earth*, 84(B6), 2995–
313 3007.
- 314 Cashman, K. V., & Kauahikaua, J. P. (1997). Reevaluation of vesicle distributions in
315 basaltic lava flows. *Geology*, 25(5), 419–422.
- 316 Clifford, S. (1986). Mars: Crustal pore volume, cryospheric depth, and the global
317 occurrence of groundwater. In *Mars: Evolution of its climate and atmosphere*
318 (Vol. 599, p. 18).
- 319 Clifford, S. (1997). The origin of the martian intercrater plains-the role of liquefac-
320 tion from impact and tectonic-induced seismicity. In *Lunar and planetary sci-*
321 *ence conference* (Vol. 28, p. 241).
- 322 Davis, R., & Haltigin, T. (2021). International mars ice mapper mission: The first
323 human exploration reconnaissance mission to mars. In *Lunar and planetary*
324 *science conference* (p. 2614).
- 325 Day-Lewis, F. D., Singha, K., & Binley, A. M. (2005). Applying petrophysical
326 models to radar travel time and electrical resistivity tomograms: Resolution-
327 dependent limitations. *Journal of Geophysical Research: Solid Earth*,
328 110(B8).
- 329 Dou, S., Nakagawa, S., Dreger, D., & Ajo-Franklin, J. (2017). An effective-medium
330 model for p-wave velocities of saturated, unconsolidated saline permafrost.
331 *Geophysics*, 82(3), EN33–EN50.
- 332 Dundas, C. M., Mellon, M. T., Conway, S. J., Daubar, I. J., Williams, K. E., Ojha,
333 L., . . . others (2021). Widespread exposures of extensive clean shallow ice in
334 the midlatitudes of mars. *Journal of Geophysical Research: Planets*, 126(3),
335 e2020JE006617.
- 336 Dvorkin, J., & Nur, A. (1996). Elasticity of high-porosity sandstones: Theory for
337 two north sea data sets. *Geophysics*, 61(5), 1363–1370.
- 338 Franzson, H., Gufinnsson, G., Helgadóttir, H., & Frolova, J. (2010). Porosity, density
339 and chemical composition relationships in altered icelandic hyaloclastites. *CRC*
340 *Press Inc.*
- 341 Gassmann, F. (1951). Über die elastizität poroser medien. *Vierteljahrsschrift der*
342 *Naturforschenden Gesellschaft in Zurich*, 96, 1–23.
- 343 Golombek, M., Grott, M., Kargl, G., Andrade, J., Marshall, J., Warner, N., . . .
344 others (2018). Geology and physical properties investigations by the insight
345 lander. *Space Science Reviews*, 214(5), 1–52.
- 346 Golombek, M., Warner, N., Grant, J., Hauber, E., Ansan, V., Weitz, C., . . . others
347 (2020). Geology of the insight landing site on mars. *Nature communications*,

- 348 11(1), 1–11.
- 349 Hanna, J. C., & Phillips, R. J. (2005). Hydrological modeling of the martian crust
350 with application to the pressurization of aquifers. *Journal of Geophysical Re-*
351 *search: Planets*, 110(E1).
- 352 Hobiger, M., Hallo, M., Schmelzbach, C., Stähler, S., Fäh, D., Giardini, D., ... oth-
353 ers (2021). The shallow structure of mars at the insight landing site from
354 inversion of ambient vibrations. *Nature communications*, 12(1), 1–13.
- 355 Kalapodis, N., Kampas, G., & Ktenidou, O.-J. (2020). A review towards the de-
356 sign of extraterrestrial structures: From regolith to human outposts. *Acta As-*
357 *tronautica*, 175, 540–569.
- 358 Karl, D., Cannon, K. M., & Gurlo, A. (2021). Review of space resources processing
359 for mars missions: Martian simulants, regolith bonding concepts and additive
360 manufacturing. *Open Ceramics*, 100216.
- 361 Lewis, K. W., Peters, S., Gonter, K., Morrison, S., Schmerr, N., Vasavada, A. R., &
362 Gabriel, T. (2019). A surface gravity traverse on mars indicates low bedrock
363 density at gale crater. *Science*, 363(6426), 535–537.
- 364 Liu, J., Li, H., Sun, L., Guo, Z., Harvey, J., Tang, Q., ... Jia, M. (2021). In-situ re-
365 sources for infrastructure construction on mars: A review. *International Jour-*
366 *nal of Transportation Science and Technology*.
- 367 Lognonné, P., Banerdt, W., Pike, W., Giardini, D., Christensen, U., Garcia, R. F.,
368 ... others (2020). Constraints on the shallow elastic and anelastic structure of
369 mars from insight seismic data. *Nature Geoscience*, 13(3), 213–220.
- 370 MacKinnon, D. J., & Tanaka, K. L. (1989). The impacted martian crust: Structure,
371 hydrology, and some geologic implications. *Journal of Geophysical Research:*
372 *Solid Earth*, 94(B12), 17359–17370.
- 373 Majmudar, T. S., & Behringer, R. P. (2005). Contact force measurements and
374 stress-induced anisotropy in granular materials. *nature*, 435(7045), 1079–1082.
- 375 Makse, H. A., Gland, N., Johnson, D. L., & Schwartz, L. (2004). Granular packings:
376 Nonlinear elasticity, sound propagation, and collective relaxation dynamics.
377 *Physical Review E*, 70(6), 061302.
- 378 Makse, H. A., Gland, N., Johnson, D. L., & Schwartz, L. M. (1999). Why effective
379 medium theory fails in granular materials. *Physical Review Letters*, 83(24),
380 5070.
- 381 Manga, M., & Wright, V. (2021). No cryosphere-confined aquifer below insight on
382 mars. *Geophysical Research Letters*, 48(8), e2021GL093127.
- 383 Mindlin, R. D. (1949). Compliance of elastic bodies in contact.
- 384 Moitra, P., Horvath, D. G., & Andrews-Hanna, J. C. (2021). Investigating the
385 roles of magmatic volatiles, ground ice and impact-triggering on a very recent
386 and highly explosive volcanic eruption on mars. *Earth and Planetary Science*
387 *Letters*, 567, 116986.
- 388 Morgan, G. A., Putzig, N. E., Perry, M. R., Sizemore, H. G., Bramson, A. M., Pe-
389 tersen, E. I., ... others (2021). Availability of subsurface water-ice resources in
390 the northern mid-latitudes of mars. *Nature Astronomy*, 5(3), 230–236.
- 391 Murphy, W. F. (1982). *Effects of microstructure and pore fluids on the acoustic*
392 *properties of granular sedimentary materials* (Unpublished doctoral disserta-
393 tion). Stanford University.
- 394 Pan, L., Quantin-Nataf, C., Tauzin, B., Michaut, C., Golombek, M., Lognonné, P.,
395 ... others (2020). Crust stratigraphy and heterogeneities of the first kilometers
396 at the dichotomy boundary in western elysium planitia and implications for
397 insight lander. *Icarus*, 338, 113511.
- 398 Piqueux, S., Buz, J., Edwards, C. S., Bandfield, J. L., Kleinböhl, A., Kass, D. M.,
399 ... Teams, T. (2019). Widespread shallow water ice on mars at high latitude-
400 sand midlatitudes. *Geophysical Research Letters*, 46(24), 14290–14298.
- 401 Rivera-Valentín, E. G., Chevrier, V. F., Soto, A., & Martínez, G. (2020). Distribu-
402 tion and habitability of (meta) stable brines on present-day mars. *Nature as-*

- 403 *tronomy*, 4(8), 756–761.
- 404 Scheller, E., Ehlmann, B., Hu, R., Adams, D., & Yung, Y. (2021). Long-term drying
405 of mars by sequestration of ocean-scale volumes of water in the crust. *Science*,
406 372(6537), 56–62.
- 407 Sharma, S. S., & Fahey, M. (2003). Degradation of stiffness of cemented calcareous
408 soil in cyclic triaxial tests. *Journal of Geotechnical and Geoenvironmental engi-*
409 *neering*, 129(7), 619–629.
- 410 Smrekar, S. E., Lognonné, P., Spohn, T., Banerdt, W. B., Breuer, D., Christensen,
411 U., ... others (2019). Pre-mission insights on the interior of mars. *Space*
412 *Science Reviews*, 215(1), 1–72.
- 413 Spohn, T., Hudson, T., Marteau, E., Golombek, M., Grott, M., Wippermann, T.,
414 ... others (2021). The insight hp 3 penetrator (mole) on mars: Soil properties
415 derived from the penetration attempts and related activities. *arXiv preprint*
416 *arXiv:2112.04438*.
- 417 Squyres, S., Aharonson, O., Arvidson, R., Bell, J., Christensen, P., Clark, B., ...
418 others (2006). Bedrock formation at meridiani planum. *Nature*, 443(7107),
419 E1–E2.
- 420 Squyres, S., Arvidson, R., Bell Iii, J., Bruckner, J., Cabrol, N., Calvin, W., ... oth-
421 ers (2004). The opportunity rover’s athena science investigation at meridiani
422 planum, mars. *science*, 306(5702), 1698–1703.
- 423 Suazo, G., Fourie, A., & Doherty, J. (2017). Cyclic shear response of cemented paste
424 backfill. *Journal of Geotechnical and Geoenvironmental Engineering*, 143(1),
425 04016082.
- 426 Sun, V. Z., Stack, K. M., Kah, L. C., Thompson, L., Fischer, W., Williams, A. J.,
427 ... others (2019). Late-stage diagenetic concretions in the murray formation,
428 gale crater, mars. *Icarus*, 321, 866–890.
- 429 Suzuki, M., Umezaki, T., & Takahara, H. (2012). Fast and cyclic shearing of ce-
430 mented sand in earthquake induced landslide. In *Proc. 15th world conference*
431 *on earthquake engineering, lisboa*.
- 432 Tanaka, K. L., Skinner Jr, J. A., Dohm, J. M., Irwin III, R. P., Kolb, E. J.,
433 Fortezzo, C. M., ... Hare, T. M. (2014). Geologic map of mars.
- 434 Vanorio, T., Prasad, M., & Nur, A. (2003). Elastic properties of dry clay mineral
435 aggregates, suspensions and sandstones. *Geophysical Journal International*,
436 155(1), 319–326.
- 437 Walton, K. (1987). The effective elastic moduli of a random packing of spheres.
438 *Journal of the Mechanics and Physics of Solids*, 35(2), 213–226.
- 439 Wang, C.-y., Manga, M., & Wong, A. (2005). Floods on mars released from ground-
440 water by impact. *Icarus*, 175(2), 551–555.
- 441 Warner, N., Golombek, M., Ansan, V., Marteau, E., Williams, N., Grant, J., ...
442 Banks, M. (2022). In situ and orbital stratigraphic characterization of the
443 insight landing site – a type example of a regolith-covered lava plain on mars.
444 *Journal of Geophysical Research: Planets*, n/a(n/a).
- 445 Wernicke, L. J., & Jakosky, B. M. (2021). Martian hydrated minerals: A significant
446 water sink. *Journal of Geophysical Research: Planets*, 126(3), e2019JE006351.
- 447 Wright, V., & Hornbach, M. (2021). The effects of 180 years of aging on the physical
448 and seismic properties of partially saturated sands. *Journal of Geophysical Re-*
449 *search: Solid Earth*, 126(6), e2020JB021341.
- 450 Zeghal, M., & El Shamy, U. (2008). Liquefaction of saturated loose and cemented
451 granular soils. *Powder Technology*, 184(2), 254–265.
- 452 Zimmer, M. A., Prasad, M., Mavko, G., & Nur, A. (2007). Seismic velocities of un-
453 consolidated sands: Part 1—pressure trends from 0.1 to 20 mpa. *Geophysics*,
454 72(1), E1–E13.
- 455 Zong, J., Stewart, R. R., Dyaur, N., & Myers, M. T. (2017). Elastic properties of
456 rock salt: Laboratory measurements and gulf of mexico well-log analysis. *Geo-*
457 *physics*, 82(5), D303–D317.